Parametric smoothing model for visco-elastic polishing tools

Dae Wook Kim,* Won Hyun Park, Hyun Kyoung An, and James H. Burge

College of Optical Sciences, University of Arizona, 1630 E. University Blvd., Tucson, Arizona 85721, USA
**letter2dwk@hotmail.com*

Abstract: A parametric smoothing model is developed to quantitatively describe the smoothing action of polishing tools that use visco-elastic materials. These materials flow to conform to the aspheric shape of the workpieces, yet behave as a rigid solid for short duration caused by tool motion over surface irregularities. The smoothing effect naturally corrects the mid-to-high frequency errors on the workpiece while a large polishing lap still removes large scale errors effectively in a short time. Quantifying the smoothing effect allows improvements in efficiency for finishing large precision optics. We define normalized smoothing factor *SF* which can be described with two parameters. A series of experiments using a conventional pitch tool and the rigid conformal (RC) lap was performed and compared to verify the parametric smoothing model. The linear trend of the *SF* function was clearly verified. Also, the limiting minimum ripple magnitude PV_{min} from the smoothing actions and *SF* function slope change due to the total compressive stiffness of the whole tool were measured. These data were successfully fit using the parametric smoothing model.

OCIS codes: (220.0220) Optics design and fabrication; (220.4610) Optics fabrication; (220.5450) Polishing.

References and links

1. R. A. Jones, "Computer control for grinding and polishing," Photon. Spectra, 34–39 (1963).
2. R. E. Wagner, and R. R. Shannon, "Fabrication of aspherics using a mathematical model for material removal," Appl. Opt. **13**(7), 1683–1689 (1974).
3. D. D. Walker, D. Brooks, A. King, R. Freeman, R. Morton, G. McCavana, and S. W. Kim, "The 'Precessions' tooling for polishing and figuring flat, spherical and aspheric surfaces," Opt. Express **11**(8), 958–964 (2003).
4. H. M. Pollicove, E. M. Fess, and J. M. Schoen, "Deterministic manufacturing processes for precision optical surfaces," in *Window and Dome Technologies VIII*, R. W. Tustison, eds., Proc. SPIE 5078, 90–96 (2003).
5. J. H. Burge, S. Benjamin, D. Caywood, C. Noble, M. Novak, C. Oh, R. Parks, B. Smith, P. Su, M. Valente, and C. Zhao, "Fabrication and testing of 1.4-m convex off-axis aspheric optical surfaces," in *Optical Manufacturing and Testing VIII*, J. H. Burge; O. W. Fähnle and R. Williamson, eds., Proc. SPIE 7426, 74260L1–12 (2009).
6. D. W. Kim, S. W. Kim, and J. H. Burge, "Non-sequential optimization technique for a computer controlled optical surfacing process using multiple tool influence functions," Opt. Express **17**(24), 21850–21866 (2009).
7. R. E. Parks, "Alignment of off-axis conic mirrors," in *Optical Fabrication and Testing*, OSA Technical Digest Series (Optical Society of America, 1980), paper TuB4.
8. N. J. Brown, and R. E. Parks, "The polishing-to-figuring transition in turned optics," SPIE's 25th Annual International Technical Symposium, (SPIE, 1981)
9. P. K. Mehta, and P. B. Reid, "A mathematical model for optical smoothing prediction of high-spatial frequency surface errors," in *Optomechanical Engineering and Vibration Control*, E. A. Derby, C. G. Gordon, D. Vukobratovich, P. R. Yoder Jr., and C. H. Zweben, eds., Proc. SPIE 3786, 447 (1999).
10. M. T. Tuell, J. H. Burge, and B. Anderson, "Aspheric optics: smoothing the ripples with semi-flexible tools," Opt. Eng. **41**(7), 1473–1474 (2002).
11. M. T. Tuell, "Novel tooling for production of aspheric surfaces," M.S. Thesis (2002).
12. M. Johns, "The Giant Magellan Telescope (GMT)," in *Extremely Large Telescopes: Which Wavelengths?* T. E. Andersen, eds., Proc. SPIE 6986, 698603 1–12 (2008).
13. J. Nelson, and G. H. Sanders, "The status of the Thirty Meter Telescope project," in *Ground-based and Airborne Telescopes II*, L. M. Stepp and R. Gilmozzi, eds., Proc. SPIE 7012, 70121A1–18 (2008).
14. A. Ardeberg, T. Andersen, J. Beckers, M. Browne, A. Enmark, P. Knutsson, and M. Owner-Petersen, "From Euro50 towards a European ELT," in *Ground-based and Airborne Telescopes*, L. M. Stepp, eds., Proc. SPIE 6267, 626725 1–10 (2006).
15. A. Heller, "Safe and sustainable energy with LIFE" (2009), *https://str.llnl.gov/AprMay09/pdfs/05.09.02.pdf*.

#133659 - $15.00 USD Received 20 Aug 2010; revised 1 Oct 2010; accepted 7 Oct 2010; published 8 Oct 2010

16. R. E. Parks, "Specifications: Figure and Finish are not enough," in *An optical Believe It or Not: Key Lessons Learned*, M. A. Kahan, eds., Proc. SPIE 7071, 70710B1–9 (2008).
17. J. M. Hill, "Optical Design, Error Budget and Specifications for the Columbus Project Telescope," in *Advanced Technology Optical Telescopes IV*, L. D. Barr, eds., Proc. SPIE 1236, 86–107 (1990).
18. D. W. Kim, and J. H. Burge, "Rigid conformal polishing tool using non-linear visco-elastic effect," Opt. Express **18**(3), 2242–2257 (2010).
19. H. M. Martin, R. G. Allen, J. H. Burge, D. W. Kim, J. S. Kingsley, M. T. Tuell, S. C. West, C. Zhao, and T. Zobrist, "Fabrication and testing of the first 8.4 m off-axis segment for the Giant Magellan Telescope," in *Modern Technologies in Space- and Ground-based Telescopes and Instrumentation*, E. Atad-Ettedgui and D. Lemke, eds., Proc. SPIE 7739, 77390A (2010).
20. M. J. Valente, D. W. Kim, M. J. Novak, C. J. Oh, and J. H. Burge, "Fabrication of 4-meter class astronomical optics," in *Modern Technologies in Space- and Ground-based Telescopes and Instrumentation*, E. Atad-Ettedgui and D. Lemke, eds., Proc. SPIE 7739, 77392D (2010).
21. R. P. Chhabra, and J. F. Richardson, *Non-Newtonian Flow and Applied Rheology (2nd edition)* (Elsevier Ltd, 2008), Chap. 1.
22. D. W. Kim, W. H. Park, S. W. Kim, and J. H. Burge, "Parametric modeling of edge effects for polishing tool influence functions," Opt. Express **17**(7), 5656–5665 (2009).
23. M. A. Meyers, and K. K. Chawla, *Mechanical Behavior of Materials (2nd edition)* (Cambridge University Press, 2009), 124–125.
24. A. C. Fischer-Cripps, "Multiple-frequency dynamic nanoindentation testing," J. Mater. Res. **19**(10), 2981–2988 (2004).
25. D. W. Kim and J. H. Burge of the College of Optical Sciences, University of Arizona, 1630 East University Boulevard, Tucson, AZ 85721 are preparing a manuscript to be called "Smoothing performance of various polishing tools."
26. B. C. Don Loomis, Crawford, Norm Schenck, and Bill Anderson, Optical Engineering and Fabrication Facility, University of Arizona, 1630 E. University Blvd, Tucson, Arizona 85721, (personal communication, 2009).
27. N. J. Brown, "Optical polishing pitch," in *Optical Fabrication and Testing*, Optical Society of America Workshop (Optical Society of America, 1977).

1. Introduction

Various computer controlled optical surfacing (CCOS) processes have been developed since the 1960s [1–5]. These CCOS processes provide attractive solutions for fabrication of precision optics including large aspheric optical surfaces and off-axis segments by exhibiting high convergence rates based on deterministic material removal processes [3–5].

One of the key components for a CCOS process is the polishing tools, which make the physical contact with the workpiece and removes material from it. A tool influence function (TIF) is the shape of the wear function created by the polishing tool motion (*e.g.* spin or orbital motion) on the workpiece. In general, a dwell time map optimization approach is used to achieve a given target removal map [3–6]. Optimization intelligence (*i.e.* software) uses TIFs as building blocks to achieve the target removal map by spatially distributing and accumulating them [6]. Thus, having stable and deterministic TIFs is a critical part to achieving successful CCOS processes.

The TIF is a strong function of tool properties, such as pressure distribution under the tool, polishing material at the contacting interface, contact area shape, tool motion, and so forth. For instance, developing a tool with a deterministic TIF for aspheric (or freeform) optics fabrication becomes a complex problem. Because local surface shape (*e.g.* curvature) of an aspheric surface varies as a function of position on a workpiece [7], a tool with a fixed surface shape cannot be used. Some flexibility in the tool is required to maintain intimate contact with the workpiece surface. However, rigidity of the tool is also desired to get natural smoothing effects, which removes mid-to-high spatial frequency errors on the workpiece [8–11]. Thus, a well-behaved tool development is a balancing problem between flexibility and rigidity.

The smoothing effect becomes more important for large workpiece fabrications, because it is almost the only way to correct mid-to-high spatial frequency errors smaller than the tool size. Based on the deterministic TIFs of CCOS processes, large errors (*i.e.* low spatial frequency surface errors compared to the tool size) can be corrected by increasing the dwell time on the high error areas. However, this method cannot be used for regions smaller than the tool size unless smaller and smaller tools are utilized. Smaller tools require higher tool positioning accuracy to avoid residual tool marks, which is another source of mid-spatial frequency errors. Also, the use of small tools increases the total fabrication time.

#133659 - $15.00 USD Received 20 Aug 2010; revised 1 Oct 2010; accepted 7 Oct 2010; published 8 Oct 2010

Correcting these mid-to-high spatial frequency errors on optical surfaces is very important for the next generation of extremely large telescopes such as the Giant Magellan Telescope [12–14] and for nuclear fusion energy plants using high power lasers (*e.g.* Laser Inertial Fusion Engine [15]). Because the mid-to-high-spatial frequency errors are directly related to the sharpness of the point spread function (*e.g.* Airy disk radius) or the scattering characteristic of high power laser application optics, the overall performance of those systems may be degraded due to those errors. In fact, most recent large optical surfaces have been polished to a target structure function or power spectrum density, which quantify the target form accuracy as a function of spatial frequencies [16,17].

There have been some quantitative investigations for the smoothing effects by semi-flexible tools. Brown and Parks quantitatively explained the smoothing effects by elastic backed flexible lapping belts in 1981 [8]. The smoothing effect using a large flexible polishing lap was introduced and mathematically studied by Mehta and Reid using the Bridging model [9]. The Bridging model was further developed using Fourier series decomposition approach by Tuell [10,11]. These models were successfully demonstrated with experimental data. More detailed explanation about the Bridging model will be given in Section 2.3.

A rigid conformal (RC) lap using a visco-elastic non-Newtonian fluid was developed and introduced in a previous study [18–20]. (*Note:* A US provisional patent was filed for the RC lap.) A schematic structure of the RC lap is compared with other tool types in Fig. 1 [18]. Because the storage modulus of the visco-elastic material is a function of the applied stress frequency, the smoothing effect by the RC lap has to be described by a new smoothing model [18]. Also, the new model needs to include other effects such as the fluid dynamics of the polishing compound and the total effective stiffness of the whole tool structure.

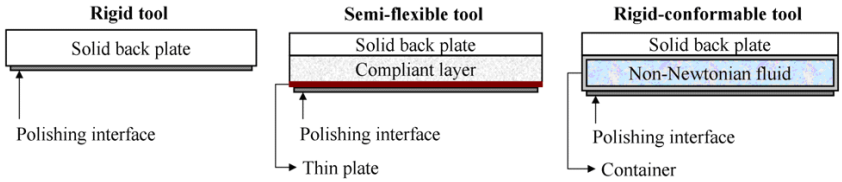

Fig. 1. Schematic tool structures of three different tool types [18].

A parametric smoothing model was developed to quantitatively describe the smoothing efficiency of visco-elastic polishing tools such as pitch tools and RC laps. Some theoretical backgrounds about the RC lap and Bridging model for semi-flexible tools are provided in Section 2. The parametric smoothing model developed based on the Bridging model is introduced in Section 3. Experimental results for the smoothing effects by a conventional pitch tool and a RC lap are provided and compared in Section 4.

2. Theoretical background

2.1 Rigid conformal lap

The RC lap, which takes advantages from both rigid and compliant tools in two different time scales using a visco-elastic non-Newtonian fluid, has been introduced and used on highly aspheric optical surfaces [18–20]. The overall structure of the lap is shown in Fig. 2.

The flow characteristic of the RC lap depends on the frequency of applied stress [21]. Because the tool motion (*e.g.* orbital motion [22]) is usually fast (*e.g.* 60 RPM) relative to the local features (*e.g.* bumps or ripples) under the motion, the RC lap acts like a rigid tool with respect to that time scale. If the tool is orbiting at 60 RPM on a bumpy area, the tool quickly smoothes out the bumps with high local pressures on the bump peaks.

#133659 - $15.00 USD Received 20 Aug 2010; revised 1 Oct 2010; accepted 7 Oct 2010; published 8 Oct 2010

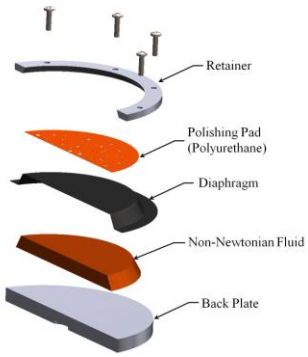

Fig. 2. 3D RC lap structure (exploded and cut in half) [18].

However, the tool will fit the overall local curvature changes on the workpiece since the RC lap moves slowly on the workpiece (*e.g.* ~1 rpm workpiece rotation) along the tool path. For instance, a 330mm diameter RC lap has been successfully used on the 8.4m off-axis segment for the Giant Magellan Telescope, which requires the tool to fit the slowly varying local curvature as it travels on the highly aspheric workpiece [19].

2.2 Smoothing by a rigid tool

The smoothing effects by a rigid tool in Fig. 1 (left) can be understood in a simple way. If we assume the tool does not fit to the surface irregularity under the tool (*i.e.* infinite rigidity), and maintains its shape, the tool only rubs the highs on the surface as shown in Fig. 3 (left). As the tool runs on the workpiece, it will wear down the highs, and eventually the surface will be smoothed out. The spatial frequency of the final surface will be directly related to the tool size of the rigid tool as shown in Fig. 3 (right). This process is clearly shown in the accompanying movie clip (Media 1).

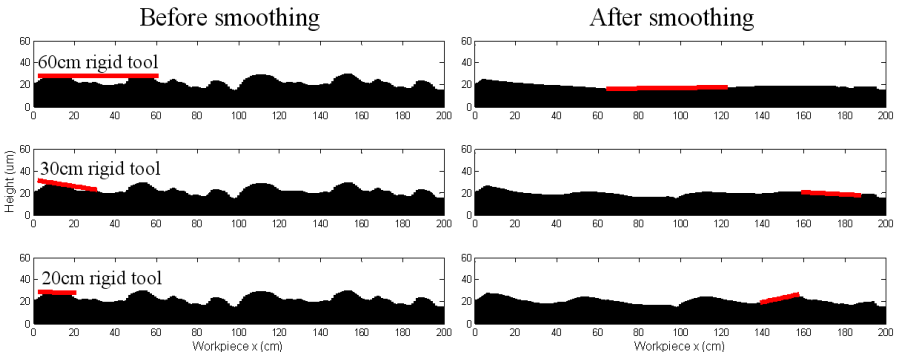

Fig. 3. Smoothing effect simulation using an infinitely rigid tool (Media 1).

Actual polishing tools, however, always require a certain amount of flexibility to fit the overall surface as briefly mention in Section 1. Also, no tool is infinitely rigid. These facts lead us to a more comprehensive smoothing model for the flexible tools in Section 2.3.

2.3 Bridging model for smoothing effects by flexible tools

One of the most common approaches to achieving a balance between flexibility and rigidity is using semi-flexible tools as shown in Fig. 1 (middle). It usually uses a relatively thin metal plate as a tool base, so that the plate's low order bending modes are used to fit the workpiece local curvatures. A foam layer is often placed between the thin plate and another base structure (*e.g.* thick plate). A polishing pad (*e.g.* polyurethane pad) or pitch is used under the semi-flexible thin plate as a polishing interface material.

#133659 - $15.00 USD Received 20 Aug 2010; revised 1 Oct 2010; accepted 7 Oct 2010; published 8 Oct 2010

In order to describe the smoothing effects by semi-flexible tools, the Bridging model was introduced [9]. As the tool moves on the workpiece, it continuously bends by different amounts to fit the local curvature, resulting in continuous changes in the pressure distribution under the tool. If a semi-flexible tool meets mid-spatial frequency ripples, the tool contacts the ridges of highs in the surface with higher pressure, and begins to smooth them out. The lap may be imagined to form a bridge across the ridges known as the bridging effect [9].

For a semi-flexible tool, the strains induced from the thin plate bending influence the polishing pressure distribution. Kirchhoff's thin plate equations were modified to include the effect of transverse shear strain. For the one-dimensional case, the polishing pressure distribution *p(x)* due to the sinusoidal error *error(x)* on the surface can be derived based on the theory of elasticity as

$$error(x) = PV(1-\sin(2\pi \cdot \xi \cdot x)), \tag{1}$$

$$P(x) = P_{nominal} + \frac{error(x)}{\frac{1}{D_{plate} \cdot (2\pi\xi)^4} + \frac{1}{D_{s\_plate} \cdot (2\pi\xi)^2} + \frac{1}{\kappa_{total}}}, \tag{2}$$

where PV is the peak-to-valley magnitude of the sinusoidal error, ξ is the spatial frequency of the surface error, $P_{nominal}$ is the nominal pressure under the tool, D_{plate} is the flexural rigidity of the plate, D_{s_plate} is the transverse shear stiffness of the plate, and κ_{total} is the compressive stiffness of the whole tool including elastic material (*e.g.* pitch) and polishing interface material (*e.g.* polyurethane pad) [9]. The flexural rigidity and transverse shear stiffness of the flexible thin plate are defined as

$$D_{plate} = E_{plate} \cdot {t_{plate}}^3 / 12(1-{\nu_{plate}}^2), \tag{3}$$

$$D_{s\_plate} = E_{plate} \cdot t_{plate} / 2(1-\nu_{plate}), \tag{4}$$

where E_{plate} is the Young's modulus of the plate material, t_{plate} is the plate thickness, and ν_{plate} is the Poisson's ratio of the plate.

The Bridging model in Eq. (2) describing the smoothing effects by a semi-flexible tool was successfully demonstrated by comparison with experimental results [9].

3. Parametric smoothing model

3.1 Dynamic modulus

The dynamic modulus values were used in the parametric smoothing model for the visco-elastic tools such as pitch or RC laps. Pitch can be regarded as an extreme of visco-elastic materials. It almost acts like a solid during the tool motion time period (*e.g.* ~seconds). However, for very long time periods (*e.g.* ~hours), it flows to fit the surface. The dynamic modulus quantitatively describes these time-dependent characteristics. It is defined as the ratio of the stress to strain under an oscillating stress condition

Two dynamic modulus values, tensile storage modulus and loss modulus, are defined as Eq. (5) and (6). The storage modulus is related to the elastic deformation, and the loss modulus is related to the time-dependent viscous behavior of a non-Newtonian fluid.

$$Storage\ modulus: E' = \frac{\sigma_0}{\varepsilon_0}\cos\delta, \tag{5}$$

$$Loss\ modulus: E'' = \frac{\sigma_0}{\varepsilon_0}\sin\delta, \tag{6}$$

where the oscillating stress and strain are expressed as

#133659 - $15.00 USD Received 20 Aug 2010; revised 1 Oct 2010; accepted 7 Oct 2010; published 8 Oct 2010

$$\varepsilon = \varepsilon_0 \sin(t\omega), \tag{7}$$

$$\sigma = \sigma_0 \sin(t\omega + \delta) \ . \tag{8}$$

The ε is the time dependent strain, ε_0 is magnitude of the strain, t is time, ω is angular frequency of the oscillation, σ is the time dependent stress, σ_0 is magnitude of the stress, and δ is phase lag between the stress and strain [23].

The phase lag δ is a function of the angular frequency ω for the non-Newtonian fluid. For an ideal solid, the strain and stress are oscillating in phase (*i.e.* δ = 0°). If the material is an ideal viscous fluid, the stress is 90° out of phase (*i.e.* δ = 90°) with the strain. A loss tangent, which is the ratio between the storage and loss modulus, is a convenient measure of the relative contribution of the solid-like and fluid-like mechanical responses [24]. The loss factor tanδ is defined as

$$\tan\delta = \frac{E''}{E'} \ . \tag{9}$$

For instance, tanδ >1 indicates a fluid-like behavior of the non-Newtonian material. If tanδ <1, it means that the solid-like response is dominant over the fluid-like response. Thus, for efficient smoothing actions, the RC lap needs to be run under conditions where tanδ <<1.

Some measured storage modulus and loss tangent values for fused silica and Silly-Putty™ (SP) by Crayola LLC were obtained from the literature [24], and are presented in Fig. 4.

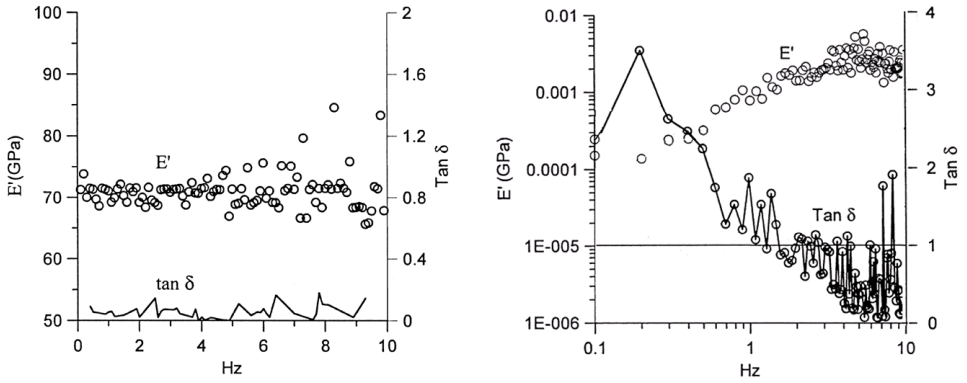

Fig. 4. Storage modulus *E´* and loss factor *tanδ* for fused silica (left) and Silly-Putty™ (right) as a function of applied stress frequency from the literature [24].

Because Fused silica can be regarded as an elastic solid, the loss tangent is almost zero. Also, the storage modulus is almost a constant ~70GPa over the 0-10Hz oscillating stress frequencies. In contrast, for the visco-elastic non-Newtonian fluid SP, the frequency dependence of the storage modulus is clearly shown in Fig. 4 (right). The SP begins to act like a solid (*i.e.* tanδ <1) when the applied stress frequency is larger than ~1Hz [24].

3.2 Polishing pressure distribution

The polishing pressure distribution under the visco-elastic tools were derived based on the Bridging model. Because there is no flexible thin plate in the tool, the Bridging model in Eq. (2) can be simplified as

$$P(x) = P_{nominal} + \kappa_{total} \cdot error(x). \tag{10}$$

Because the elastic material (*i.e.* visco-elastic material under the tanδ <<1 condition) is a part of the total compressive stiffness of the tool, the κ_{total} can be approximated by two springs connected in series as

#133659 - $15.00 USD Received 20 Aug 2010; revised 1 Oct 2010; accepted 7 Oct 2010; published 8 Oct 2010

$$\frac{1}{\kappa_{total}} = \frac{1}{\kappa_{elastic}} + \frac{1}{\kappa_{others}}, \tag{11}$$

where $\kappa_{elastic}$ is the stiffness of the elastic material and κ_{others} is the combined stiffness of all other structures including polishing pad, polishing compound fluid, wrapping material, and so forth.

By combining Eq. (10) and (11) the pressure distribution under the RC lap is expressed as

$$P(x) = P_{nominal} + \kappa_{total} \cdot error(x) = P_{nominal} + \frac{1}{\frac{1}{\kappa_{elastic}} + \frac{1}{\kappa_{others}}} \cdot error(x) \ . \tag{12}$$

The stiffness of the elastic material $\kappa_{elastic}$ can be expressed in terms of the storage modulus from Section 3.1, which defines the local pressure caused by the deformation from a bump on the workpiece. If an elastic material with storage modulus E' has a thickness L and is compressed by a ΔL tall bump, the compressive stiffness $\kappa_{elastic}$ is

$$\kappa_{elastic} = \frac{\sigma_0}{\Delta L} = \frac{\varepsilon_0 \cdot E'/\cos\delta}{\Delta L} = \frac{\{\Delta L / L\} \cdot E'/\cos\delta}{\Delta L} = \frac{E'}{L \cdot \cos\delta}, \tag{13}$$

based on Eq. (5).

The applied stress angular frequency ω is determined by the spatial frequency of the surface error ξ and the speed of the tool motion V_{tool_motion} as

$$\omega = \frac{2\pi}{T} = \frac{2\pi}{(1/\xi \cdot V_{tool\_motion})} = 2\pi \cdot \xi \cdot V_{tool\_motion}, \tag{14}$$

where T is the time interval between a position under the tool sees two adjacent peaks in the sinusoidal ripple and V_{tool_motion} is the speed of the tool motion.

For example, a RC lap with L = 8mm thick SP may rub on a sinusoidal ripple with spatial frequency ξ = 0.085mm^{-1} and ripple magnitude PV = 1μm. A typical 2500Pascal (*i.e.* ~0.36PSI) nominal pressure is assumed, and κ_{others} is ignored in this example. If the tool motion was a 20RPM orbital motion with 30mm orbital radius, the speed V_{tool_motion} is

$$V_{tool\_motion} = \frac{2\pi \cdot 30 \cdot 20}{60} = 62.8\,[mm/\sec] \ . \tag{15}$$

Then, the applied stress frequency ω in Eq. (14) becomes

$$\omega = 2\pi \cdot \xi \cdot V_{tool\_motion} = 2\pi \cdot 0.083 \cdot 62.8 = 32.77\ [radians/sec] \ . \tag{16}$$

From the measured storage modulus values in Fig. 4 (right), SP has E' = ~0.003GPa storage modulus at $f = \omega/2\pi$ = 32.77/2π = ~5Hz. The phase lag δ is almost zero, because the loss tangent tanδ is ~0 at 5Hz. Thus, using Eq. (12) and (13), the polishing pressure under the RC lap is

$$\begin{aligned} P(x) = P_{nominal} + \frac{E'}{L \cdot \cos\delta} \cdot error(x) &\approx 2500 + \frac{0.003 \times 10^9}{8 \times 10^{-3} \cdot 1} \cdot 1 \times 10^{-6} \cdot (1 - \sin(2\pi \cdot 0.085 \cdot x)) \\ &= 2500 + 375 \cdot (1 - \sin(2\pi \cdot 0.085 \cdot x))\ [Pascal], \end{aligned} \tag{17}$$

where cosδ was approximated as 1 for δ = ~0.

Thus, the high peaks on the sinusoidal surface feel an additional 375Pascal polishing pressure, which results in smoothing on the peaks.

3.3 Parametric smoothing model

In most smoothing cases, the practical interest is not in the polishing pressure distribution itself, but in the speed of the smoothing action using the pressure distribution on a given ripple

#133659 - $15.00 USD Received 20 Aug 2010; revised 1 Oct 2010; accepted 7 Oct 2010; published 8 Oct 2010

as shown in Fig. 5. This can be modeled by using the pressure distribution in the well-known Preston's equation

$$\Delta z(x) = R_{Preston} \cdot P(x) \cdot V_{tool\_workpiece}(x) \cdot \Delta t(x), \tag{18}$$

where Δz is the integrated material removal from the workpiece surface, $R_{Preston}$ is the Preston coefficient (*i.e.* removal rate), P is the polishing pressure, $V_{tool\_workpiece}$ is the relative speed between the tool and workpiece and Δt is the dwell time.

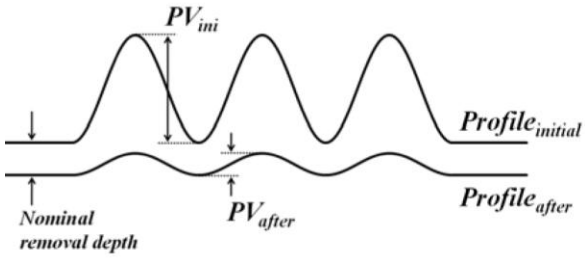

Fig. 5. The sinusoidal ripple profiles (before and after smoothing), which shows the values to determine the smoothing factor *SF* in Eq. (22).

For a given initial sinusoidal ripple magnitude PV_{ini}, the additional polishing pressure P_{add} on the peak is

$$P_{add} = P - P_{nominal} = \frac{1}{\frac{1}{\kappa_{elastic}} + \frac{1}{\kappa_{others}}} \cdot PV_{ini}, \tag{19}$$

from Eq. (12). Then, for a dwell time Δt, the decrease in the ripple magnitude ΔPV is calculated using Eq. (18) as

$$\Delta PV = PV_{ini} - PV_{after} = R_{Preston} \cdot P_{add} \cdot V_{tool\_workpiece} \cdot \Delta t \quad . \tag{20}$$

In order to normalize ΔPV, the nominal removal depth (*i.e.* removal depth from the nominal pressure) is used as

$$nominal\_removal\_depth = R_{Preston} \cdot P_{nominal} \cdot V_{tool\_workpiece} \cdot \Delta t \quad . \tag{21}$$

Using Eq. (19), (20) and (21), the smoothing factor *SF* is defined as

$$SF \equiv \frac{\Delta PV}{nominal\_removal\_depth} = \frac{1}{P_{nominal} \cdot (\frac{1}{\kappa_{elastic}} + \frac{1}{\kappa_{others}})} \cdot PV_{ini} \quad . \tag{22}$$

This definition for the smoothing factor in Eq. (22) turns out to be very useful, because it can be expressed as a linear function in *SF vs.* PV_{ini} space. For instance, the smoothing efficiency (*i.e.* the ripple magnitude decrease per unit nominal removal depth) can be easily calculated for a given initial ripple magnitude.

Because the real smoothing effect may be affected by other complex factors such as polishing pads, wrapping materials (*e.g.* the diaphragm in Fig. 2) and the fluid dynamics of polishing compounds, the theoretical smoothing model in Eq. (22) was parameterized using two parameters, C_1 and C_2, to fit the measured data. The first parameter C_1 represents κ_{others} and other unknown effects which may change the slope of the linear *SF* function. As the PV_{ini} becomes smaller and smaller the fluid dynamics of the polishing compound may begin to limit the smoothing action. This can give a limiting minimum ripple magnitude PV_{min} of the ripple, which means no more smoothing occurs below PV_{min}. This can be represented as an x-intercept C_2 in *SF vs.* PV_{ini} space.

The resulting parametric smoothing model is

#133659 - $15.00 USD Received 20 Aug 2010; revised 1 Oct 2010; accepted 7 Oct 2010; published 8 Oct 2010

$$SF \equiv \frac{1}{P_{nominal} \cdot \left(\frac{1}{\kappa_{elastic}(\omega)} + \frac{1}{C_1}\right)} \cdot (PV_{ini} - C_2), \tag{23}$$

where C_1 is the slope correction parameter and C_2 is the x-intercept parameter. Because this is a linear function, these two parameters can be easily determined in practice by performing a few smoothing runs using a given polishing tool.

We acknowledge that, at the other extreme range where the *PV* becomes large, the polishing tool may not fully deform to the ripple (*i.e.* partial contact [9]) and only touch some high portions of the ripple. Thus, beyond a certain PV_{max}, *SF* function is not a function of PV_{ini} anymore, but will be a constant.

In summary, the smoothing factor *SF* was defined to describe the smoothing effect. For a given polishing tool the smoothing efficiency is conveniently represented by a linear function in *SF vs.* PV_{ini} space. In order to include some unknown factors, which affect the smoothing action, the smoothing model was parameterized with two parameters.

4. Experimental verification of the parametric smoothing model

4.1 Experimental set-up

Sets of smoothing experiments comparing smoothing efficiencies for various polishing cases (*e.g.* Gugolz 64 *vs.* 73 pitch tool) were performed. A part of the experimental results confirming the validity of the linear parametric smoothing model is presented in this manuscript. The whole experimental results will be provided in a separate paper with detailed comparisons and discussions [25].

Two sets of experiments using a conventional pitch tool and a RC lap were performed. Because a pitch tool is known for its superb smoothing effect, it is a good reference for the smoothing efficiency comparison [26]. Details of the experimental set-up are provided in Table. 1.

Table 1. Experimental set-up for the smoothing experiment

	Pitch tool	RC lap
Tool diameter	100mm	100mm
Aluminum back plate thickness	20mm	20mm
Elastic material	Gugolz 73 pitch	Pink Silly-Putty™
Elastic material thickness, *L*	8mm	8mm
Polishing interface	Pitch itself	1.3mm thick LP-66 (polyurethane)

A sinusoidal ripple with spatial frequency $\xi = 1/12 = 0.085\text{mm}^{-1}$ and *PV* = ~0.4μm was generated on 250mm diameter Pyrex workpieces as shown in Fig. 6 (right). A specially designed pitch tool was used to generate the ripples as shown in Fig. 6 (left). This ripple generating pitch tool was made by pressing the warm pitch tool on a plastic mandrel board with many grid holes. By gently stroking the ripple generating pitch tool on the workpieces, sinusoidal ripples were generated without sharp cliff-like features in the ripple, which could have limited the measurement accuracy (*e.g.* the unwrapping problem of a phase shifting interferometric test).

#133659 - $15.00 USD Received 20 Aug 2010; revised 1 Oct 2010; accepted 7 Oct 2010; published 8 Oct 2010

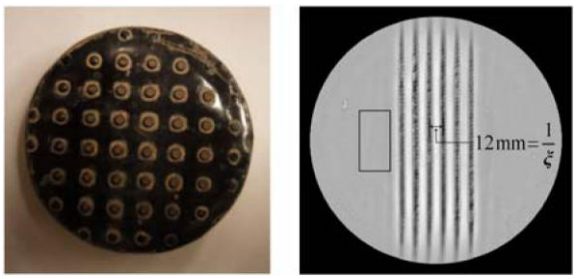

Fig. 6. The ripple generating pitch tool with a grid of circles (left) and a grey scale surface map of the Pyrex substrate with sinusoidal ripples and reference area to measure the nominal removal depth in a rectangular box (right).

The pitch tool and RC lap were run with an orbital tool motion on the workpieces. The change of the ripple magnitude, ΔPV, and the nominal removal depth in the rectangular reference area in Fig. 6 (right) were measured. These experiments were repeated until the magnitude of the ripples did not decrease anymore (*i.e.* the end of the smoothing effect). More detail of the tool operating condition is presented in Table. 2.

Table 2. Operating condition for the pitch tool and RC lap

Workpiece	250mm diameter Pyrex
Tool motion	Orbital tool motion (w/ 30mm orbital radius)
Tool motion RPM	20-30RPM
Nominal tool pressure	2500 Pascal (*i.e.* 0.36PSI)
Polishing compound	Rhodite 906 (Cerium based)
Polishing compound particle size	~2μm

Based on the pitch tool and RC lap information in Table 1 and 2, the compressive stiffness $\kappa_{elastic}$ for the parametric smoothing model was calculated using Eq. (13) as

$$Pitch\ tool: \quad \kappa_{elastic} = \frac{E'}{L \cdot \cos\delta} = \frac{2.5 \times 10^9}{8 \times 10^3 \cdot 1} = 312500 \ [Pa/\mu m], \tag{24}$$

$$RC\ lap: \quad \kappa_{elastic} = \frac{E'}{L \cdot \cos\delta} = \frac{0.003 \times 10^9}{8 \times 10^3 \cdot 1} = 375 \ [Pa/\mu m], \tag{25}$$

and used in the parametric smoothing model, Eq. (23). For the storage modulus (*i.e.* Young's modulus) of the pitch tool, a typical value 2.5 GPa was assumed [27]. The actual storage modulus of the pitch is a function of many factors such as the temperature of pitch. This uncertainty becomes a part of the first parameter C_1 in the parametric smoothing model. Also, pitch is practically a solid within the orbital tool motion time scale. Thus, the phase lag δ was assumed as 0. The RC lap was stroked at 20 RPM in the experiments in order to evaluate the smoothing efficiency while the tool is used in the solid-like state. As shown in Section 3.2, for the 20RPM orbital motion, storage modulus E' is 0.003GPa and the phase lag δ is ~0.

4.2 Measured smoothing factor for pitch tool and RC lap

The ripples on the workpiece were measured using a Fizeau interferometer. Because the actual ripples were not ideal sinusoidal curves, an averaged peak-to-valley value using >90% and <90% height values was used to calculate the *PV*. Some measured profiles are presented in Fig. 7 as an example. The decrease in ripple magnitude as the smoothing time gets longer is clearly shown. The pitch tool (left) smoothes out the ripples much quicker than the RC lap (right).

#133659 - $15.00 USD Received 20 Aug 2010; revised 1 Oct 2010; accepted 7 Oct 2010; published 8 Oct 2010

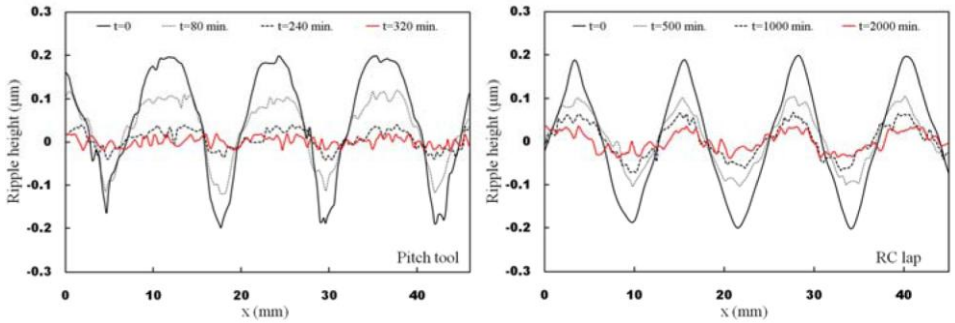

Fig. 7. Measured ripple profiles as tool smoothes out the ripples: pitch tool (left) and RC lap (right) [18]. (*Note:* The initial ripple magnitude *PV* was about 0.4μm for both cases.)

The measured ΔPV values were normalized by the measured nominal removal depth to calculate the smoothing factor *SF* as explained in Section 3.3. The experiments were performed until no more reduction in the ripple magnitude (*i.e.* smoothing factor $SF = \sim 0$) was observed. The experimental results are plotted in Fig. 8.

Two parameters C_1 and C_2 in the parametric smoothing model were used to fit the measured data as shown in Fig. 8. The first parameter C_1 was used to match the slope of the data. The second parameter C_2 was used to match the x-intercept of the data, which is the parametric representation of the smoothing limit PV_{min} mentioned in Section 3.3.

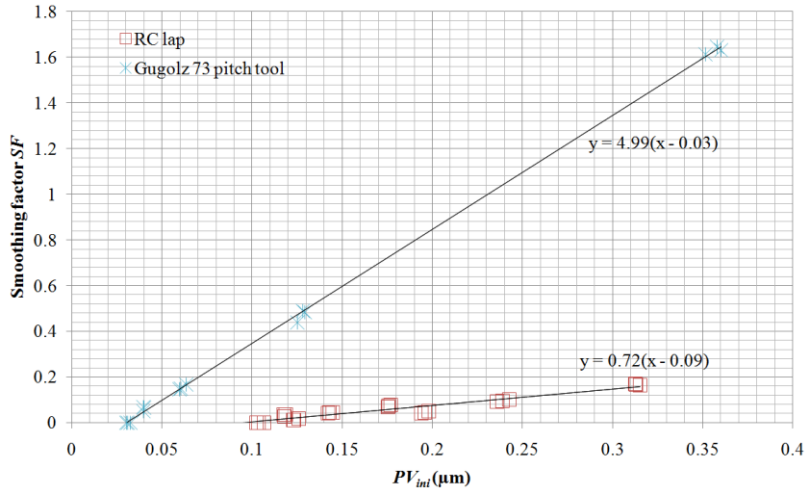

Fig. 8. Measured smoothing factor *SF vs.* initial ripple magnitude P_{ini} for pitch tool and RC lap. (*Note:* The solid line represents the linear fit using the parametric smoothing model. Two parameters C_1 and C_2 were used to fit the measured data as shown in Table 3.)

The fitted parameter values are presented in Table 3 with the calculated compressive stiffness $\kappa_{elastic}$ values from Eq. (24) and (25). The linear trend predicted by the parametric smoothing model in Eq. (23) was successfully verified. The C_1 for the pitch tool case was much smaller (~0.04 times) than the compressive stiffness $\kappa_{elastic}$ of the pitch, so that the slope of the parametric *SF* function was smaller than the slope solely based on the pitch stiffness itself. One possible explanation for this result may be the polishing compound liquid layer between the pitch surface and the workpiece, which may change the total compressive stiffness. However, the pitch tool still shows ~7 times more efficient (*i.e.* ~7 times steeper *SF* slope) smoothing action than the RC lap. The limiting magnitude of the ripple PV_{min} was measured experimentally and fitted using the second parameter C_2. The pitch tool was able to smooth out the ripples down to $PV_{min} = \sim 0.03$μm.

#133659 - $15.00 USD Received 20 Aug 2010; revised 1 Oct 2010; accepted 7 Oct 2010; published 8 Oct 2010

Table 3. Compressive stiffness $\kappa_{elastic}$ and two parameter values for parametric smoothing model

	$\kappa_{elastic}$ (Pa/μm)	C_1 (Pa/μm)	C_2 (μm)
Pitch tool	312500	12994	0.03
RC lap	375	–474	0.09

In contrast, the C_1 for the RC lap was a negative number. This may result from the under-estimated $\kappa_{elastic}$ of the RC lap. The actual $\kappa_{elastic}$ of the pink SP may be different from the value based on the literature [24]. Also, the polyurethane pad and wrapping material in the RC lap may change the total compressive stiffness of the tool. These unknowns were absorbed in the parameter C_1 to evaluate the smoothing efficiency of the RC lap. The PV_{min} was measured and fitted using C_2. The RC lap smoothed out the ripples down to PV_{min} = ~0.09μm. Changing the thickness L of the elastic material is expected to result in a steeper SF function, because $\kappa_{elastic}$ is a function of L as shown in Eq. (13). These additional modalities including different orbital motion RPM, which changes the applied stress frequency, will be reported in a separate study [25] as mentioned above.

5. Concluding remarks

A parametric smoothing model was developed to quantitatively describe the smoothing efficiency. A convenient normalized smoothing factor SF was defined using two parameters for the parametric smoothing model. A series of experiments were performed to verify the parametric smoothing model. The linear trend of the SF function was clearly verified by the experimental results. The limiting ripple magnitude PV_{min} from the smoothing actions and change of slope due to the total compressive stiffness of the whole tool structure were also measured and successfully fitted using those two parameters.

The RC lap, which showed a highly deterministic removal rate (*i.e.* <10% stability) and superb surface finish (*e.g.* <1nm RMS surface roughness) [18], can be used more efficiently with the known smoothing factor for large precision optics fabrications [19,20]. It will contribute to the realization of some next generation optical systems which usually have hundreds of meter-class aspheric mirrors (*e.g.* Thirty Meter Telescope [13] and Laser Inertial Fusion Engine [15]) or large off axis mirrors (*e.g.* 8.4meter Giant Magellan Telescope mirrors [12,19]).

Acknowledgments

We acknowledge that this work was supported by the Optical Engineering and Fabrication Facility of the College of Optical Sciences at the University of Arizona. We thank Marty Valente (Optical Engineering and Fabrication Facility), Hubert Martin (Steward Observatory Mirror Lab), Fan Bin (Institute of Optics and Electronics) and Brian Cuerden (Steward Observatory) for assistance in the final manuscript preparation. The measured data in Fig. 4 was available in this manuscript with the permission of the Journal of Materials Research. We thank the journal and A. C. Fischer-Cripps, the author of the original manuscript.

#133659 - $15.00 USD Received 20 Aug 2010; revised 1 Oct 2010; accepted 7 Oct 2010; published 8 Oct 2010